Numerical Analysis of a New Nonlinear Twist Extrusion Process

Tuncay Yalçinkaya [1],* , Ülke Şimşek [1], Hiroyuki Miyamoto [2] and Motohiro Yuasa [2]

[1] Department of Aerospace Engineering, Middle East Technical University, Ankara 06800, Turkey; ulke.simsek@metu.edu.tr
[2] Department of Mechanical Engineering, Doshisha University, Kyotanabe city, Kyoto 610-0321, Japan; hmiyamot@mail.doshisha.ac.jp (H.M.); myuasa@mail.doshisha.ac.jp (M.Y.)
* Correspondence: yalcinka@metu.edu.tr; Tel.: +90-312-2104258

check for
updates

Abstract: Severe plastic deformation (SPD) can produce ultrafine grained (UFG) and nanocrystalline (NC) materials by imposing intense plastic strain. One of the many options for inducing large plastic strains is to pass the material through a torsional/twist extrusion. The high-strength materials fabricated by SPD has no limit in dimension, and they can even be applied to load-carrying structural materials. Even though the method is quite successful, the industrial transfer has been limited so far because of low production efficiency and high cost. To remedy such difficulties, a new torsional extrusion process called nonlinear twist extrusion (NLTE) is introduced in this study, which has been designed based on two principles; (1) linear arrangement of the production line and (2) effective die geometry resulting in higher and more homogeneous plastic strain evolution which would give better grain refinement. The initial computational study of the designed geometry for the new extrusion process is addressed in the current study. The obtained results are discussed in detail with respect to conventional extrusion process, which is referred to as linear twist extrusion (LTE). The method is expected to offer a great potential for industrial use.

Keywords: SPD; twist extrusion; grain refinement

1. Introduction

Heavy deformation of metallic materials for the purpose of obtaining alloys with improved properties has centuries of history. In this context, the work of Bridgman [1] started a new era where intrinsically rather brittle metals were subjected to large deformation under high pressures to improve the mechanical properties. Since then this approach, which has been regarded as the severe plastic deformation (SPD) method, has been of great interest worldwide for materials science community from both scientific and practical standpoints. SPD can produce ultrafine grained (UFG) materials in a bulk form through simple processes and do not need complicated thermomechanical treatments [2]. Equal-channel angular pressing (ECAP) (see e.g., [3–5]), high-pressure torsion (HPT) (see e.g., [6]), and accumulative roll bonding (ARB) (see e.g., [7–9]) are the typical and well-known SPD methods, which has been studied for the last 20–30 years. The disadvantage of these typical SPD methods is batch processing, and therefore commercial production by industry has been very limited for the high production cost. The continuous processing which can be applied to long bars or plates is essential to apply SPD to the commercial production of structural materials in various fields. Modified SPD for the continuous process has been proposed such as conshearing [10], equal-channel angular drawing [11], continuous confined strip shearing [12], ECAP-conform, twist extrusion (TE) [13], simple shear extrusion (SSE) [14,15]. Among the continuous SPD methods, the straight movement of bars in TE and SSE methods is the advantage for the commercialization in that they can be installed in a conventional

mass production system with low cost. However, the advantage of the straight movement of bars is the disadvantage in view of effective deformation routes for grain fragmentation because of limited deformation route. In both methods, a shear strain of positive and negative sense is coupled in the channel [16]. In SPD processing, UFG formation is facilitated in deformation routes which involve high dislocation accumulation, and strain reversal or redundant strain reduces the rate of the dislocation accumulations and hence retard the UFG formation (see e.g., [17,18]).

The classical TE processes, which is referred to as the linear twist extrusion (LTE) is based on pressing out a prism specimen through a die with a profile consisting of two prismatic regions separated by a twist part (see e.g., [19–22]). The original cross-section is maintained while it undergoes SPD and the process can be applied repeatedly, which changes in the microstructure and properties of the specimen. High backpressure is applied when it exits the die. A disadvantage of LTE is strain localization at the inlet and outlet of the twisting part. Very high strain is imposed to the billet at both parts while the billet is subjected to rigid body rotation inside the twisting part. This local strain causes high punching force and possibly inhomogeneous strain distribution.

The current study proposes a new SPD technique called Nonlinear Twist Extrusion (NLTE) to overcome the disadvantages of LTE process. The preliminary experimental observations have been addressed for pure magnesium recently in [23]. In this work the initial numerical analysis is presented in comparison to classical TE processes, focusing on the advantages which will lead to effective grain refinement. NLTE technique is devised based on TE, but in here an effective die geometry is designed resulting in higher and more homogeneous plastic strain evolution. The shear strain is imposed throughout the whole channel without rigid body rotation. The purpose is to spread the high plastic deformation to the larger regions of the cross-section.

The paper is organized as follows. First, in Section 2, the theoretical aspects of kinematics and the kinetics of the NLTE process is discussed. Then in Section 3, the die geometry for both linear and NLTE is introduced, and the numerical procedure is summarized. The material response, boundary conditions, and finite element analysis procedure are presented. The numerical results for both linear and nonlinear cases are illustrated in comparison in Section 4. The results are discussed in detail. Finally, the work is summarized and concluding remarks are given in Section 5.

2. Kinetics and Kinematics of NLTE Process

Assume that the rotation angle of twist channel and displacement can be expressed as $\theta = Cx^n$. θ is the rotation angle by twisting, C is basically γ/r, x is the displacement along the longitudinal axis, n is the parameter, which is 1 for the linear torsion case (see Figure 1).
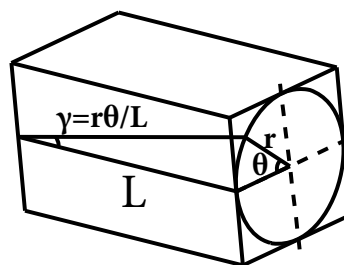

Figure 1. Linear twisting geometry.

In the conventional TE, the rotation angle can be assumed to increase linearly with displacement. Therefore, it can be written as $\frac{d\theta}{dx} = C$, and for $n = 2$ (e.g., for NLTE) the rotation angle θ increases in a parabolic relation and it can be found that $\frac{d\theta}{dx} = 2Cx$. It shows that the workpiece rotates more in NLTE process than the LTE. As a consequence, for a nonlinear design it is expected that specimen must be faced with more severe and homogeneous plastic deformation if it is compared with LTE process.

The currently designed channel of NLTE consists of three parts as shown in Figure 2. In part I, the cross-section of the channel changes gradually from a circular of the radius r to elliptical shape with the major and minor axes of a and b, respectively. Since $ab = r^2$, the cross sectional area of the channel is constant through this part. In part II, the bar is twisted according to the parabolic relation $\theta = Cx^2$. In part III, the twisting continues with a constant rotation angle, but the cross-section changes from elliptical to circular shape again. Note that the change of twisting rate at the sections between the part I and II is smooth so that a rapid increase of shear strain and resulting stress concentration are avoided. Similarly, the billet is extruded out of the die keeping the rotation so that the strain reversal is avoided. In LTE, the shear strain is localized and strain reversal are imposed to the billet, which retard the grain fragmentation. FEM simulations illustrate that a backpressure is necessary for a proper extrusion process resulting in the original cross-section. Equivalent plastic strain values are used to show the advantage of the NLTE process with respect to LTE one. By using the equivalent plastic strain relations and by considering three parts of deformation of NLTE, the equivalent plastic strain part I from circle (r) and to ellipse (a, b; $ab = r^2$) can be found as follows;

$$d\varepsilon_I^{eq} = \sqrt{\frac{2}{3}[(d\varepsilon_x^p)^2 + (d\varepsilon_y^p)^2 + (d\varepsilon_z^p)^2 + \frac{1}{3}((d\gamma_{xy}^p)^2 + (d\gamma_{zx}^p)^2 + (d\gamma_{yz}^p)^2)]} \tag{1}$$

In the first part of NLTE, when the following conditions of $d\varepsilon_z^p = d\gamma_{xy}^p = d\gamma_{yz}^p = d\gamma_{xz}^p = 0$, $d\varepsilon_x^p = \frac{dx}{r}$ and $d\varepsilon_y^p = \frac{dy}{r}$ are applied, then the equivalent plastic strain in part I is;

$$d\varepsilon_I^{eq} = \sqrt{\frac{2}{3}[(\frac{dx}{r})^2 + (\frac{dy}{r})^2]} = \sqrt{\frac{2}{3}(\frac{dx}{r})^2 + (\frac{-dx}{r})^2} = \frac{2}{\sqrt{3}}\frac{dx}{r} \tag{2}$$

$$\varepsilon_I^{eq} = \int_r^a d\varepsilon_I^P = \frac{2}{\sqrt{3}}\ln\frac{a}{r} \tag{3}$$

Equivalent strain part II in NLTE can be described below;

$$d\varepsilon_{II}^{eq} = \sqrt{\frac{2}{3}[(d\varepsilon_r^p)^2 + (d\varepsilon_\theta^P)^2 + (d\varepsilon_x^p)^2 + \frac{1}{3}[(d\gamma_{r\theta}^p)^2 + (d\gamma_{xr}^p)^2 + (d\gamma_{\theta x}^p)^2]]} \tag{4}$$

Within the part II $d\varepsilon_r^{eq} = d\varepsilon_\theta^P = d\gamma_{\theta x}^p = d\gamma_{xr}^p = 0$ and $d\gamma_{r\theta}^p = rCdx$

$$\varepsilon_{II}^{eq} = \int \varepsilon_{II}^p = \sqrt{\frac{1}{3}}\int d\gamma_{r\theta}^p = \sqrt{\frac{1}{3}\frac{r\theta_{max}}{L}} \tag{5}$$

Since the deformations in part I and part III are similar, the equivalent strains are the same. Finally, the equivalent plastic strain (peq) equation for NLTE is shown below;

$$\varepsilon^{eq} = 2\varepsilon_I^p + \varepsilon_{II}^P \tag{6}$$

$$\varepsilon^{eq} = 2(\frac{2}{\sqrt{3}}\ln\frac{a}{r}) + \sqrt{\frac{1}{3}\frac{r\theta_{max}}{L}} \tag{7}$$

According to Equation (7) for one pass of NLTE specimen, the equivalent plastic strain is approximately 1.4. As it will be shown in the following section the value of the back pressure is identified according to this value, which will depend on the material as well.
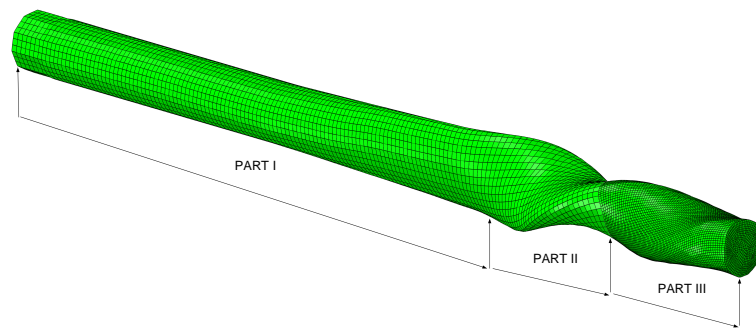
Figure 2. Schematic extrusion of the nonlinear twisting workpiece.

3. Simulations of the Linear and the Nonlinear Twist Extrusion

Commercial finite element software Abaqus is used for the simulations of LTE and NLTE processes. Copper specimens are modeled which have square and cylindrical shapes for LTE and NLTE, respectively. Von Mises plasticity model is employed as the constitutive model to simulate SPDs of workpiece. True stress-strain curve of copper specimen is illustrated in Figure 3. The dimensions of square and cylindrical specimens are 20 mm $\times$ 20 mm $\times$ 50 mm and $r = 10$ mm $\times$ 30 mm length. Due to the design complexity of the modeled die geometries and the existence of SPDs, the explicit dynamic approaches are used. In order to reduce the computational cost and to speed up the simulations mass scaling is applied in the analyses. In the current analysis the kinetic energy of the model is kept lower than the internal energy to prevent potential errors that might occur due to inertial forces. Moreover, the models have been tested and validated through simulations without mass scaling, which gives confidence in the approach. To simulate the kinetics of the process, a velocity boundary condition is applied on the punch through its rigid body definition reference point. Punch speed is 4 mm/s and friction coefficient between the die and specimen surfaces is chosen to be 0.01. This value is considerably low compared to the ones used in other SPD processes such as ECAP, yet consistent with the values used in the TE literature. To ensure the removal of specimens from the die, the dummy bodies were modeled with the same constitutive definition with specimens and they were combined to each other with their contact surfaces by using tie constraints. The die geometries, specimens and punches were modeled as rigid bodies in simulations. Mesh properties of the simulation models were given in Table 1 and FE model of the LTE and NLTE processes are shown in Figure 4. The mesh size has been obtained considering the balance between the characteristic length and the wave speed. Boundary conditions were chosen to represent experimental extrusion process. Dies and dummy dies movement and rotation degree of freedoms are restricted through their rigid body definition reference point and punch could only move through extrusion direction.

Table 1. FEM Model Mesh Parameters of simulated LTE and NLTE processes.

Model	Element Type	Element Family	Number of Elements
LTE Die	Explicit-Tetrahedral-C3D4	3D Stress	305,835
LTE Dummy Die	Explicit-Hexahedral-C3D8R	3D Stress	2538
LTE Punch	Explicit-Hexahedral-C3D8R	3D Stress	925
LTE Specimen	Explicit-Hexahedral-C3D8R	3D Stress	20,000
LTE Dummy Specimen	Explicit-Hexahedral-C3D8R	3D Stress	4500
NLTE Die	Explicit-Tetrahedral-C3D4	3D Stress	419,316
NLTE Dummy Die	Explicit-Hexahedral-C3D8R	3D Stress	19,866
NLTE Punch	Explicit-Hexahedral-C3D8R	3D Stress	1679
NLTE Specimen	Explicit-Hexahedral-C3D8R	3D Stress	48,750
NLTE Dummy Specimen	Explicit-Hexahedral-C3D8R	3D Stress	15,794
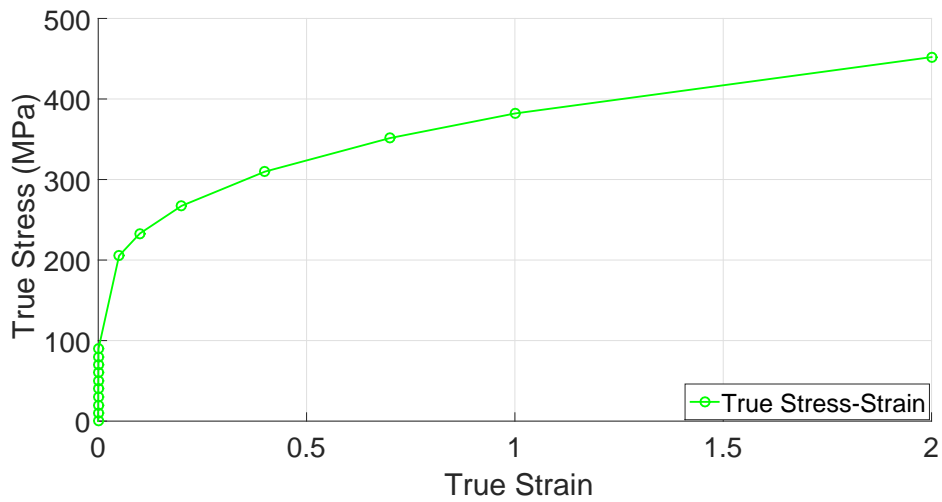
Figure 3. True Stress vs True Strain curve of copper specimen from [24].

(**a**) LTE Model

(**b**) LTE Mesh Model
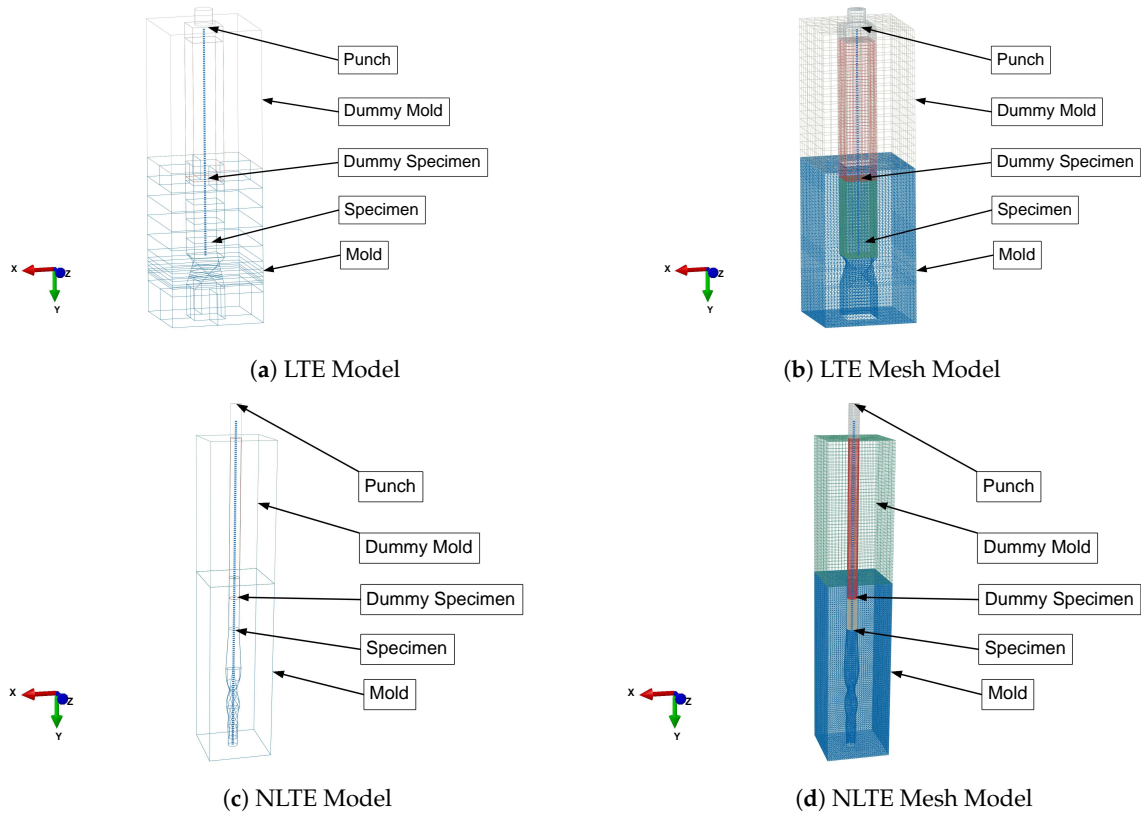
(**c**) NLTE Model

(**d**) NLTE Mesh Model

Figure 4. FEA Models of LTE and NLTE Processes.

4. Results

To compare the deformation behavior of LTE and NLTE processes, two typical elements of specimen were chosen at the inner and the outer sections of workpieces distinctively (see e.g., [25,26] for similar representation). The selected elements are highlighted in Figure 5.
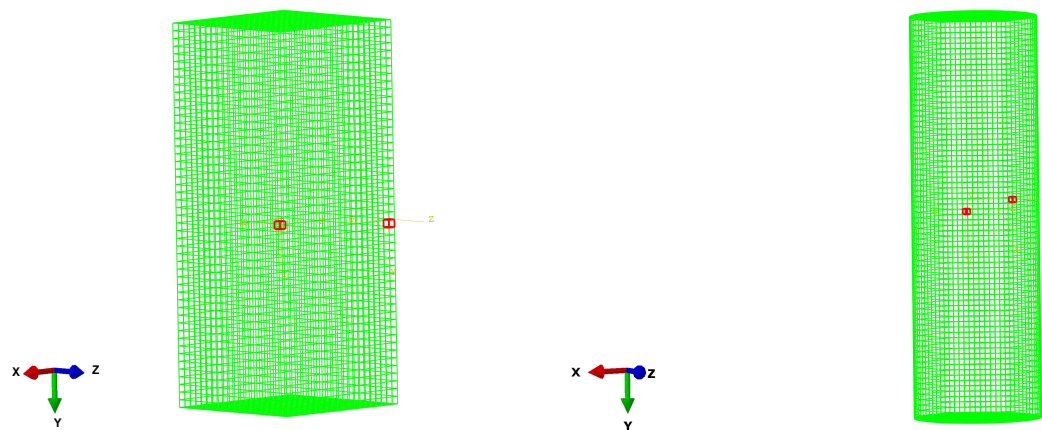
Figure 5. Investigated elements with their local coordinates at the center and the middle for LTE process (**left**) and the NLTE process (**right**).

The simulations illustrate that there is an initial sudden increase of the load in LTE when the specimen head enters the twist zone (see Figure 6). Then the work piece advances twist zone without a significant load change. This behavior has also been discussed in the previous reports (see e.g., [27]). On the contrary, in NLTE, load proceeds its increase throughout the process. This is one of the prominent advantages of NLTE. However, the punch forces are dependent on the frictional coefficient. In these calculations, the coefficient is set to be low (0.01). If it gets higher, the punch forces would increase for both processes. However, the sharp increase in the linear case is due to the sudden change in the cross-section, which does not exist in the proposed smoother nonlinear process. Since the cross-section areas are different for both cases punch pressures are compared in Figure 7 for a better presentation. Similar observation exists here as well at the initial part; however, the pressure goes up to much higher values in the case of NLTE. The force as well as the pressure could easily be reduced in the proposed nonlinear case by changing the geometry of channel (twisting rate) and the increase in the number of passes would give the desired total strain.
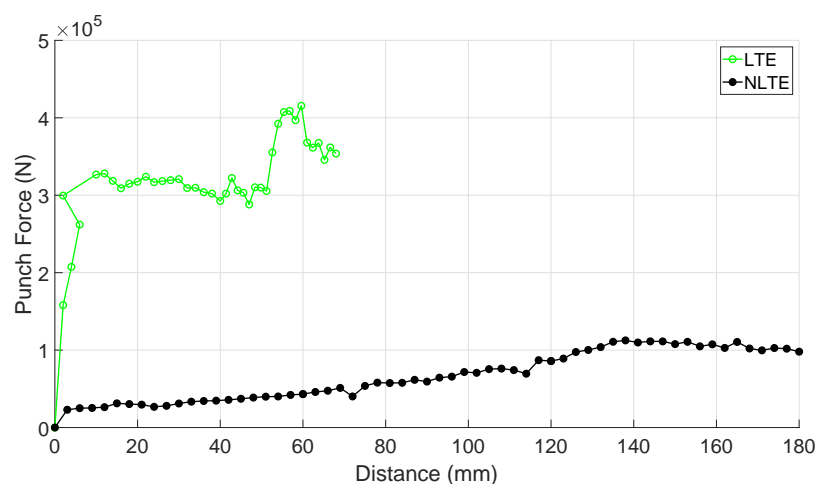

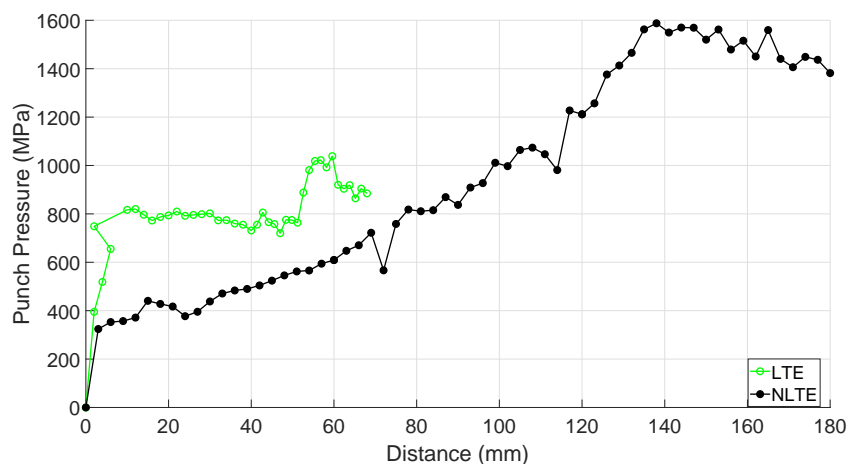**Figure 6.** The punch reaction force for both LTE and NLTE processes.

Figure 7. The punch pressure for both LTE and NLTE processes.

The deformed geometry of specimen during processes and the equivalent plastic strain distribution are directly affected by the applied back pressure (see e.g., [28]). In this context, Figures 8 and 9 show the equivalent plastic strain distribution and the change in the geometry of the specimen depending on the back pressure values. It can be seen that an increase in back pressure yields more homogenous equivalent strain distribution for both processes. The specimens fill the die better than the case without the applied back pressure. Moreover, the final cross-section shape resembles the initial geometry with the applied back pressure. This is specific to the current design due to the presented evolution of the cross-section, while in some other types of extrusion processes the effect of back pressure is not pronounced (see e.g., [29]). To decide the amount of the applied back pressure value in simulations, an approximation to the calculated theoretical equivalent plastic strain value is used here. Figure 10 shows the equivalent plastic strain distribution of inner and outer element of LTE and NLTE specimens according to various back pressure values. It can be seen that plastic equivalent strain evolution in NLTE process on the cross-section is more homogeneous compared to to traditional LTE process for various back pressure values. 200 MPa back pressure value is identified from Figure 10 to obtain the theoretical value of 1.4. Therefore, from now on this value of back pressure is applied in all FEM simulations of LTE and NLTE processes.

Von Mises stress contours are illustrated in Figure 11a,b for both LTE and NLTE processes. The stress values show an increase from the specimen center to the periphery, and maximum stresses can be observed at the edge of the surfaces. In the case of LTE stress evolution is more heterogeneous and higher stress values are obtained in certain regions. On the contrary, in the NLTE case stress distribution is more homogenous throughout the specimen and high stress values are distributed more homogeneously as well.

Figure 12 shows the equivalent plastic strain distribution in both LTE and NLTE specimens. In the case of LTE process smaller magnitude of equivalent plastic strain evolves around specimen center and there is a gradual increase from the center to the surface of the specimen. Distinctively, in case of NLTE process equivalent plastic strain evolves uniformly. The Vickers hardness data for the copper specimen which is extruded through both processes is presented in Figure 13. This experimental data proves the plastic deformation evolution on the cross-section in a qualitative way. The situation can be illustrated by using volume fraction histograms in Figure 14 as well. Volume fraction is computed as the number of elements which have the same plastic deformation interval divided by the whole element number of specimen (see e.g., [27]). Histogram shows the volume fraction of each level of plastic strain values. The LTE process has wider distribution of equivalent plastic strain distribution in histogram. On the other hand, the NLTE process has higher fraction at higher equivalent plastic strain value and more uniform distribution of equivalent plastic strain.
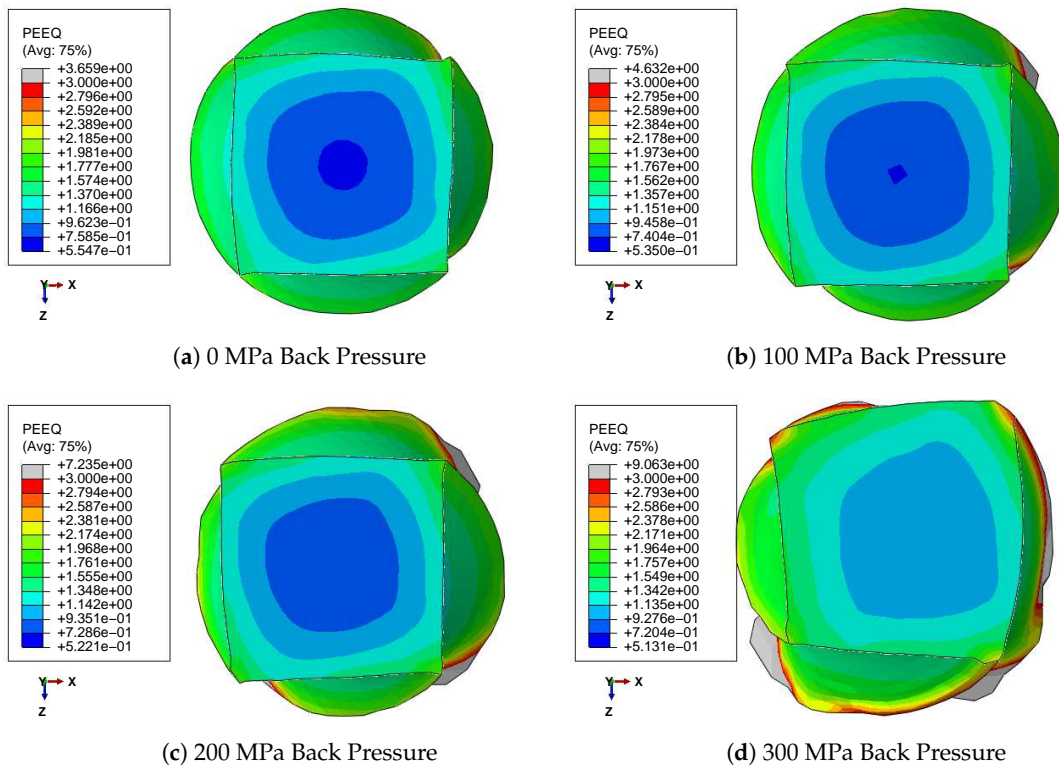
Figure 8. Equivalent plastic strain distribution in LTE specimen depending on the applied back pressure.
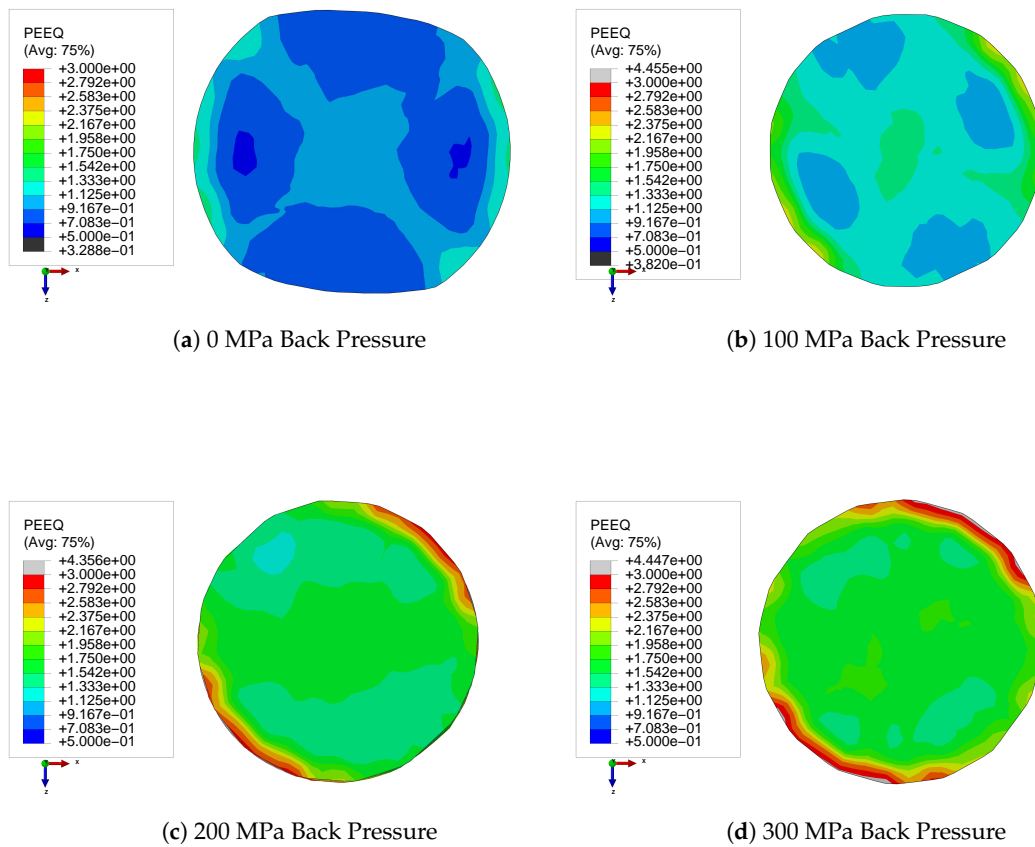

Figure 9. Equivalent plastic strain distribution in NLTE specimen depending on the applied back pressure.
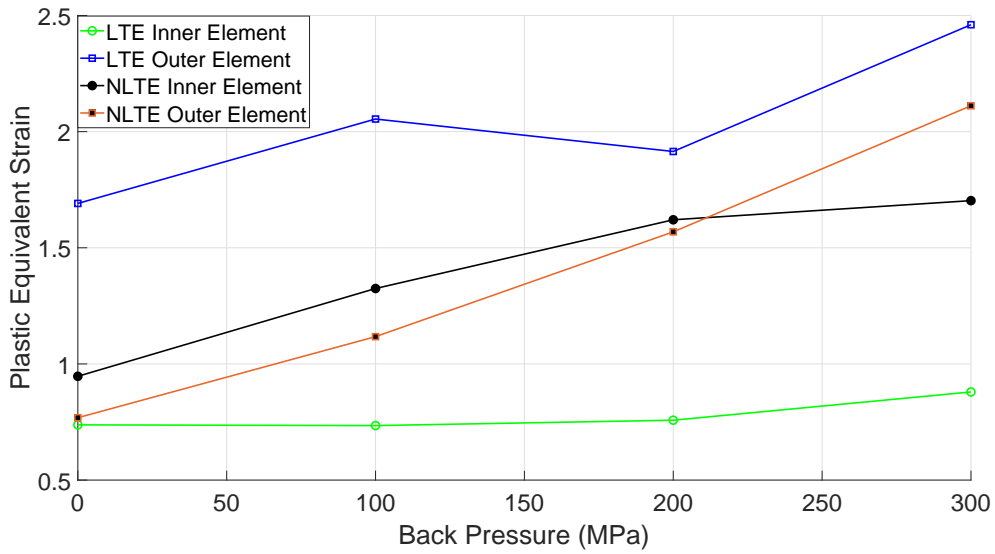
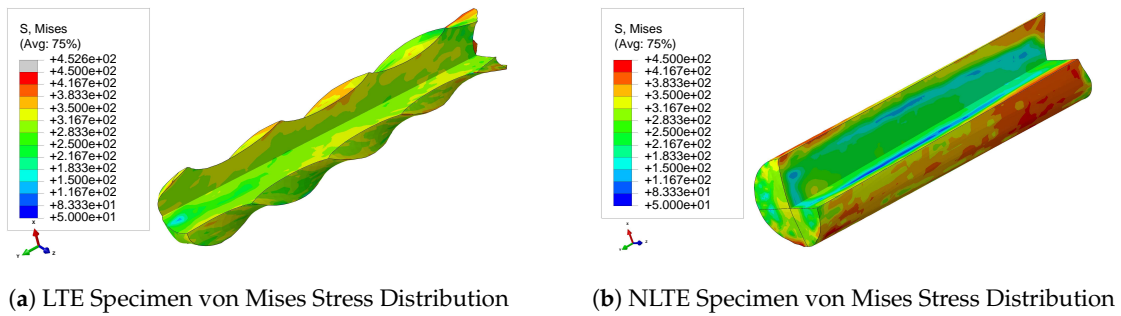**Figure 10.** The variation of equivalent plastic strain under various back pressure values.

(**a**) LTE Specimen von Mises Stress Distribution

(**b**) NLTE Specimen von Mises Stress Distribution

Figure 11. The von Mises stress distribution in LTE and NLTE specimens (MPa).

(**a**) LTE Specimen

(**b**) LTE Specimen section view

(**c**) NLTE Specimen

(**d**) NLTE Specimen section view
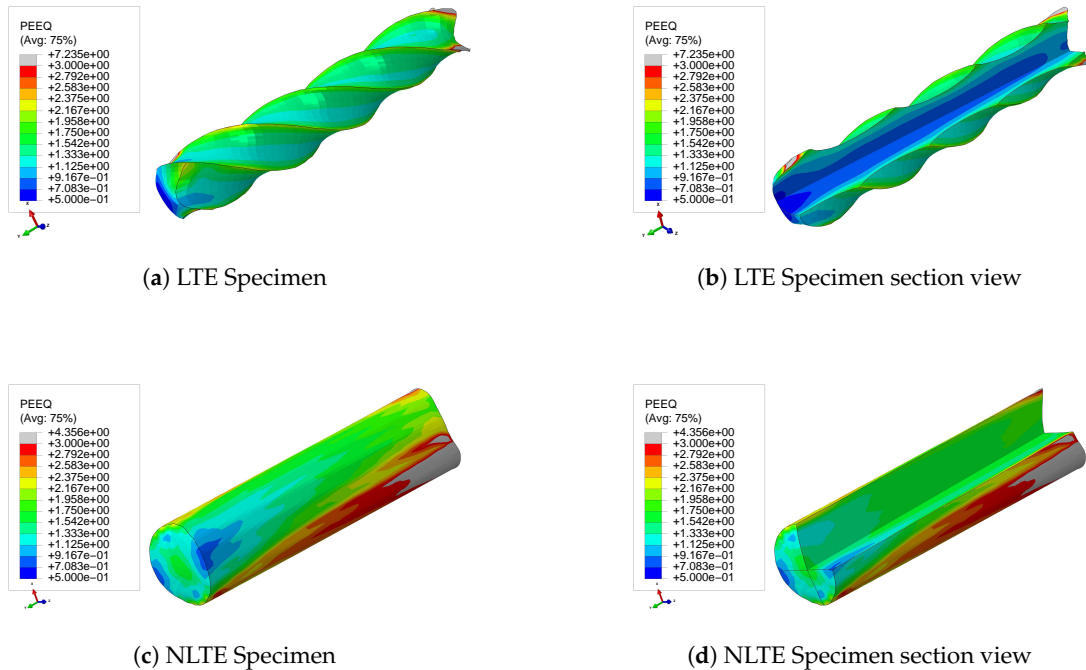
Figure 12. Equivalent plastic strain distribution in LTE and NLTE processes.

Figure 15 shows the variation of nominal plastic strains at various times during the LTE and NLTE deformation processes for outer and inner elements. The graphics were plotted according to the local coordinate systems for each typical element. In LTE process, tensional normal plastic strain evolves at the outer element in 11 direction, while the inner element shows compressive normal plastic strain. In NLTE process the deformation behavior of inner and outer elements are almost equivalent and the elements have tendency to extend.

Regarding the 22 component the LTE shows again distinct behavior and heterogeneous evolution for the inner and outer elements. Inner elements of the specimen are exposed to more nominal plastic strain than outer elements. Tensional plastic strains become effective in the inner elements throughout the process while the magnitude of outer element changes from compression to tension in 22 extrusion direction. It is noticeable that a considerably high tensional normal plastic strain evolves in inner element of LTE process. For the NLTE, the deformation characteristics of outer and inner elements are quite similar and compressive plastic strains have effect on elements in 22 extrusion direction.

For the 33 component of nominal plastic strain, it can be seen that the inner and outer elements are under compression throughout the process. A considerably high compressive nominal plastic strains are produced in the outer element during LTE process.
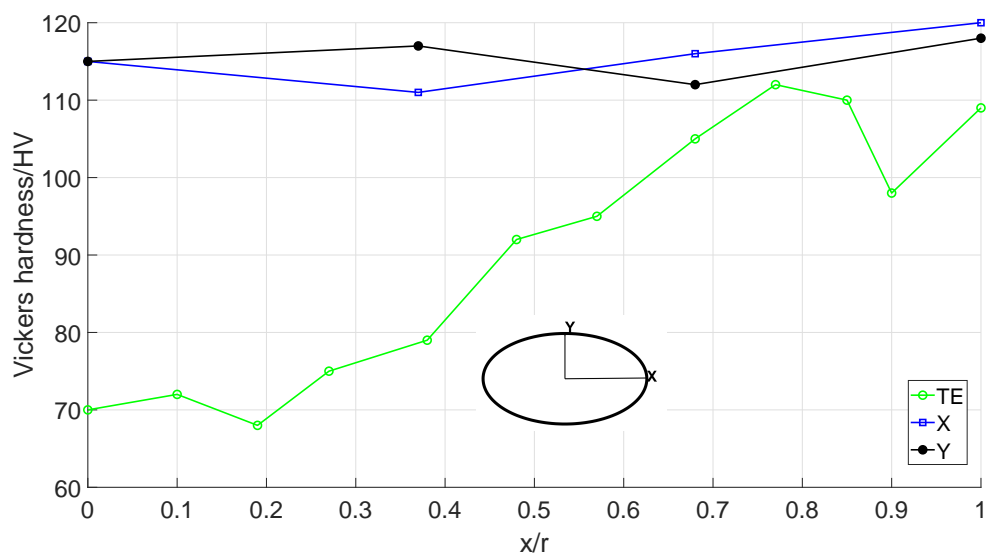

Figure 13. Vickers hardness data on the cross-section for both LTE and NLTE process.

Figure 16 shows the variation of shear plastic strain at various times during the LTE and NLTE deformation process for outer and inner elements according to each typical element's local coordinates. For the evolution of 12 and 23 components, there is a substantial difference in the outer and the inner element deformation characteristics of LTE process. It is explicitly demonstrated that high plastic strain of 1.5 is obtained in 12 direction in the outer element of LTE. For the case of NLTE the outer element experiences more plastic shear strain than the inner element. The differences are less for the 23 component. Regarding the 13 component, the variation of plastic shear strain is considerably high in NLTE process and the outer and the inner element deformation characteristics are quite similar. The outer elements experience more plastic strain for both processes. Please note that shear strain 13 of the outer element is reduced by the strain reversal in LTE while the amount of reversion is smaller in NLTE. Against the design concept of NLTE, strain reversion in NLTE occurs because of frictional force which suppress the complete rotation of the billet. The frictional force is a function of the pressure and contact area, and both are in a trade-off relation. To reduce the strain reversal in NLTE, we must design a more optimum channel of the die in terms of metal flow with less pressure and the frictional force.
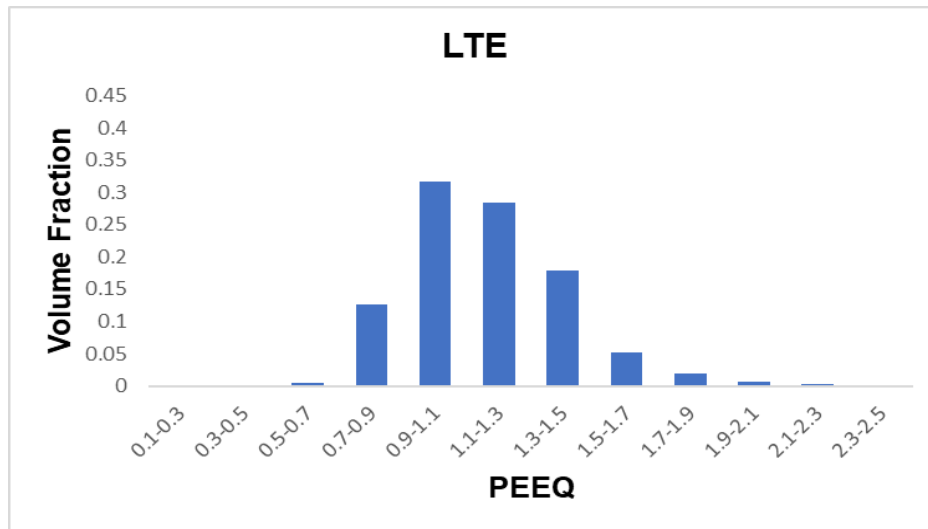
(**a**) LTE process
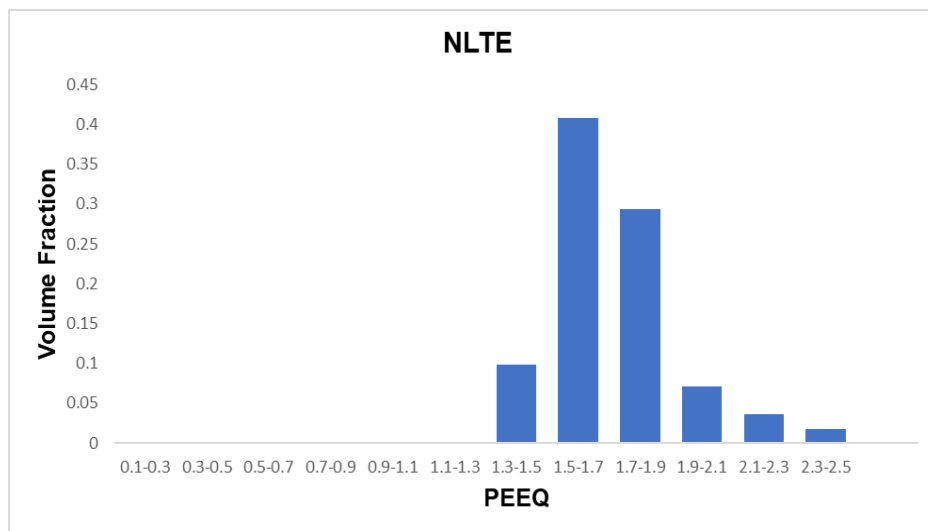
(**b**) NLTE process

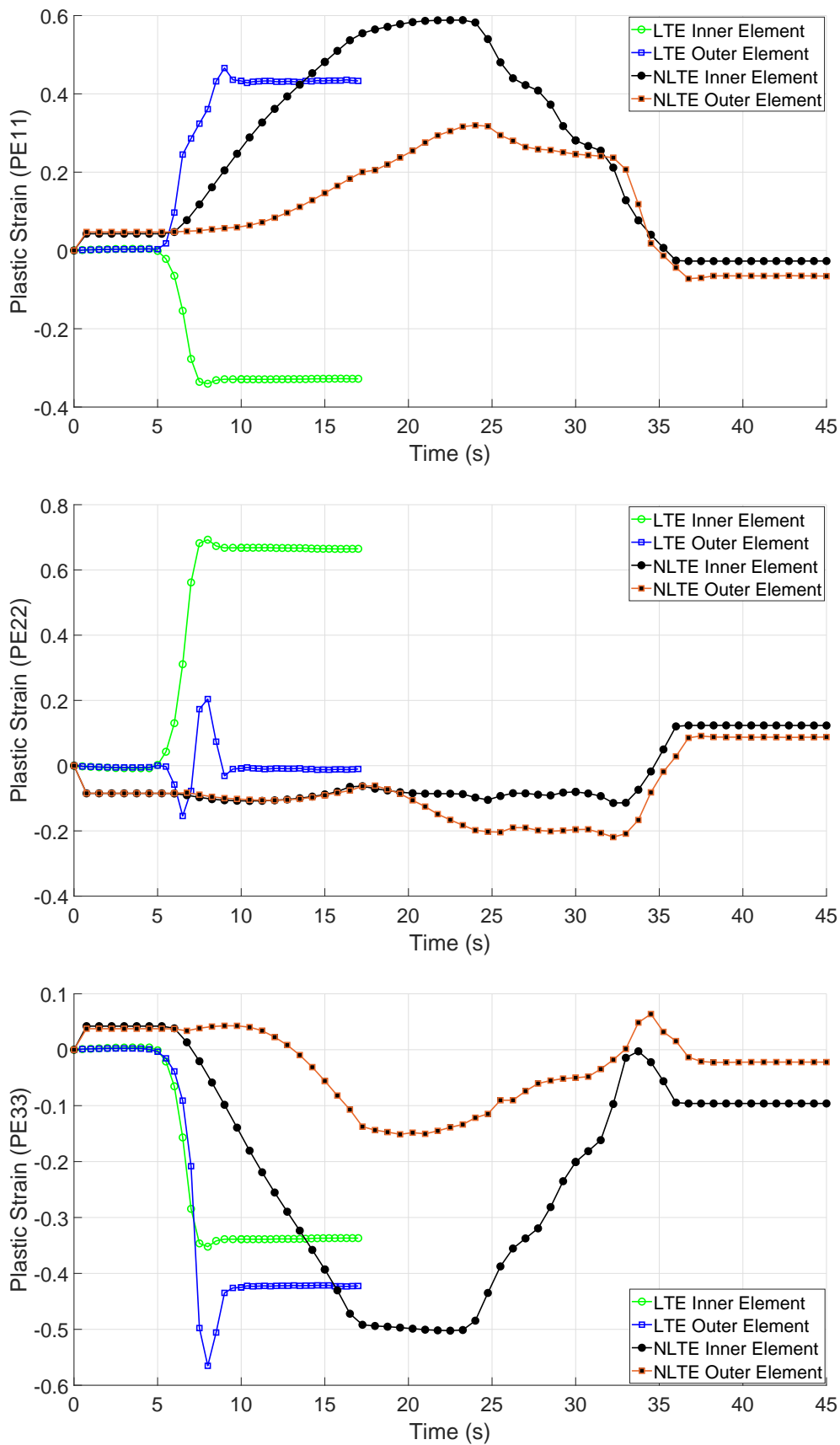**Figure 14.** Equivalent plastic strain volume fraction distribution in LTE and NLTE specimens.

Figure 15. Evolution of normal plastic strains during LTE and NLTE deformation processes at outer and inner elements.
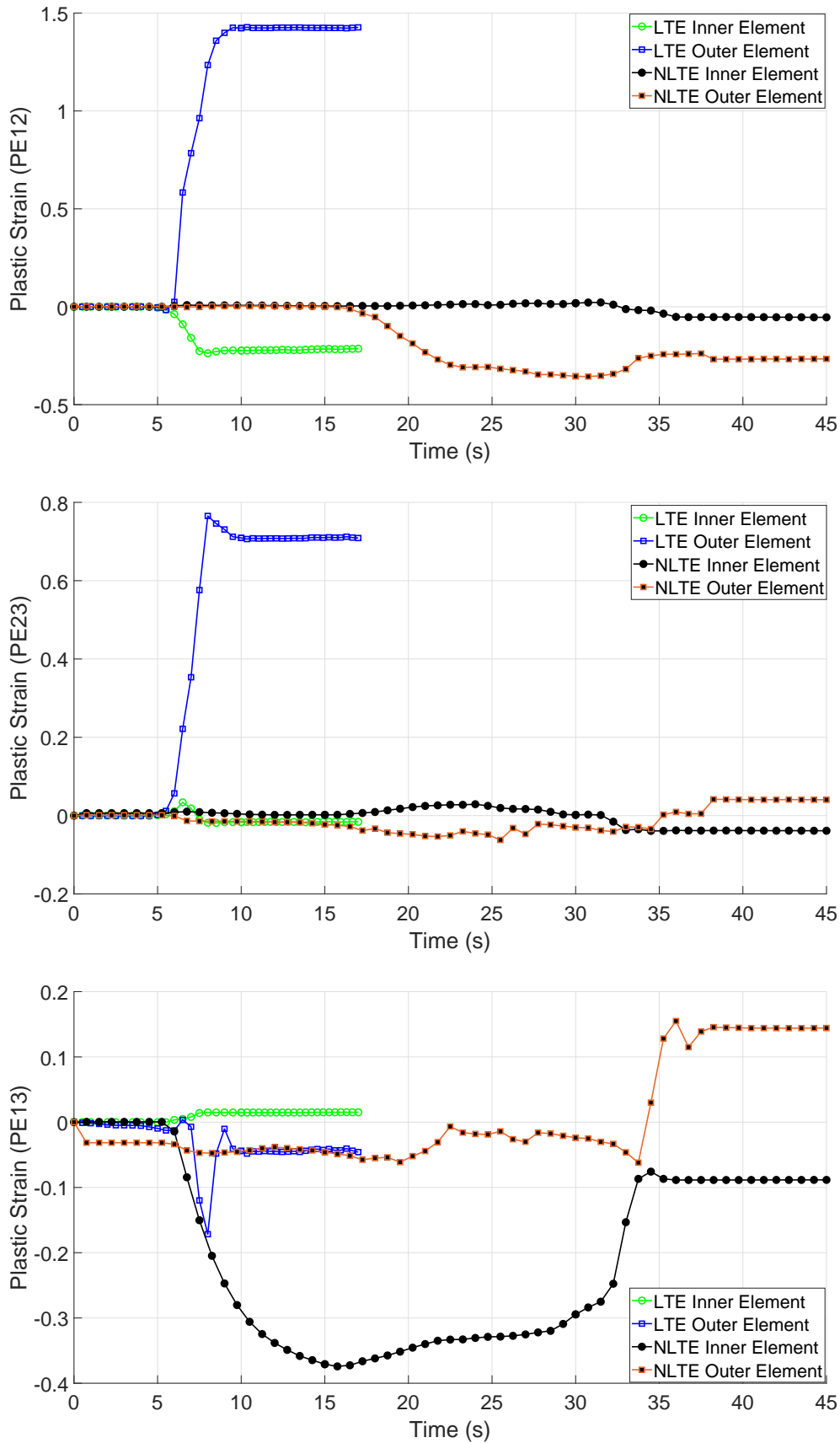
Figure 16. Evolution of shear plastic strain during the LTE and NLTE deformation processes at outer and inner elements.

5. Conclusions

This study presents a new design for the TE process to obtain more effective grain refinement procedure and to overcome the disadvantages of classical processes. The performance of the design in terms of grain refinement has been illustrated experimentally on pure magnesium in [23] and in here the first detailed numerical analysis is presented where the effectiveness of the method has been shown in terms of spatial deformation evolution during the procedure. The initial results show the advantages of the process in terms of punching force and deformation distribution, where we have obtained more pronounced strain evolution for grain refinement with less punch force. It has been illustrated also that applied back pressure has substantial influence on the final geometry and evolution of plastic strain. The obtained equivalent plastic strain values show consistency with the theoretical calculations. While the LTE process induce strain evolution increasing from inner elements to outer ones, more homogenous plastic strain distribution is captured by NLTE process. This means the later results in a more homogeneous grain refinement procedure. Moreover, equivalent plastic strain volume fraction of NLTE reaches higher values compared to LTE, which makes it more effective compared to classical processes. As a next step the experimental illustration of the design will be conducted and the texture evolution will be analyzed through crystal plasticity finite element method.

Conflicts of Interest: The authors declare no conflict of interest.

References

1.　Bridgman, P.W. *Studies in Large Plastic Flow and Fracture*;　McGraw-Hill: New York, NY, USA, 1952.
2.　Valiev, R.Z.; Langdon, T.G. Principles of Equal-Channel Angular Pressing as a Processing Tool for Grain Refinement. *Prog. Mater. Sci.* **2006**, *51*, 881–981. [CrossRef]
3.　Segal, V.M.; Reznikov, V.I.; Drobyshevskiy, A.E.; Kopylov, V.I. Plastic working of metals by simple shear. *Russ. Metall.* **1981**, *1*, 99–105.
4.　Serban, N.; Cojocaru, V.D.; Butu, M. Mechanical Behavior and Microstructural Development of 6063-T1 Aluminum Alloy Processed by Equal-Channel Angular Pressing (ECAP): Pass Number Influence. *JOM* **2012**, *64*, 607–614. [CrossRef]
5.　Serban, N.; Ghiban, N.; Cojocaru, V.D. Mechanical Behavior and Microstructural Development of 6063-T1 Aluminum Alloy Processed by Equal-Channel Angular Pressing (ECAP): Die Channel Angle Influence. *JOM* **2013**, *65*, 1411–1418. [CrossRef]
6.　Zhilyaev, A.P.; Langdon, T.G. Using high-pressure torsion for metal processing: Fundamentals and applications. *Prog. Mater. Sci.* **2008**, *53*, 893–979. [CrossRef]
7.　Saito, Y.; Tsuji, N.; Utsunomiya, H.; Sakai, T.; Hong, R. Ultra-fine grained bulk aluminum produced by accumulative roll-bonding (ARB) process. *Scr. Mater.* **1998**, *39*, 1221–1227. [CrossRef]
8.　Romberg, J.; Freudenberger, J.; Bauder, H.; Plattner, G.; Krug, H.; Hollander, F.; Scharnweber, J.; Eschke, A.; Kuhn, U.; Klauss, H.; et al. Ti/Al Multi-Layered Sheets: Accumulative Roll Bonding (Part A). *Metals* **2016**, *6*, 30. [CrossRef]
9.　Romberg, J.; Freudenberger, J.; Watanabe, H.; Scharnweber, J.; Eschke, A.; Kuhn, U.; Klauss, H.; Oertel, C.G.; Skrotzki, W.; Eckert, J.; et al. Ti/Al Multi-Layered Sheets: Differential Speed Rolling (Part B). *Metals* **2016**, *6*, 31. [CrossRef]
10.　Utsunomiya, H.; Saito, Y.; Suzuki, H.; Sakai, T. Development of the continuous shear deformation process. *Proc. Inst. Mech. Eng. Ser. B* **2001**, *215*, 947–957. [CrossRef]

11. Zisman, A.A.; Rybin, V.V.; Van Boxel, S.; Seefeldt, M.; Verlinden, M.B. Equal Channel Angular Drawing of Aluminium Sheet. *Mater. Sci. Eng. A* **2006**, *427*, 123–129. [CrossRef]

12. Lee, J.C.; Seok, H.K.; Suh, J.Y. Microstructural evolutions of the Al strip prepared by cold rolling and continuous equal channel angular pressing. *Acta Mater.* **2002**, *50*, 4005–4019. [CrossRef]

13. Orlov, D.; Beygelzimer, Y.; Synkov, S.; Varyukhin, V.; Horita, Z. Evolution of Microstructure and Hardness in Pure Al by Twist Extrusion. *Mater. Trans.* **2008**, *49*, 2–6. [CrossRef]

14. Pardis, N.; Ebrahimi, R. Deformation behavior in Simple Shear Extrusion (SSE) as a new severe plastic deformation technique. *Mater. Sci. Eng. A* **2009**, *527*, 355–360. [CrossRef]

15. Bagherpour, E.; Reihanian, M.; Ebrahimi, R. On the capability of severe plastic deformation of twining induced plasticity (TWIP) steel. *Mater. Des.* **2012**, *36*, 391–395. [CrossRef]

16. Latypov, M.I.; Yoon, E.Y.; Lee, D.J.; Kulagin, R.; Beygelzimer, Y.; Seyed Salehi, M.; Kim, H.S. Microstructure and Mechanical Properties of Copper Processed by Twist Extrusion with a Reduced Twist-Line Slope. *Metall. Mater. Trans. A* **2014**, *45*, 2232–2241. [CrossRef]

17. Iwahashi, Y.; Horita, Z.; Nemoto, M.; Langdon, T. An investigation of microstructural evolution during equal-channel angular pressing. *Acta Mater.* **1997**, *45*, 4733–4741. [CrossRef]

18. Wetscher, F.; Pippan, R. Cyclic high-pressure torsion of nickel and Armco iron. *Philos. Mag.* **2006**, *86*, 5867–5883. [CrossRef]

19. Beygelzimer, Y.; Varyukhin, V.; Synkov, S.; Orlov, D. Useful properties of twist extrusion. *Mater. Sci. Eng. A* **2009**, *503*, 14–17. [CrossRef]

20. Beygelzimer, Y.; Prilepo, D.; Kulagin, R.; Grishaev, V.; Abramova, O.; Varyukhin, V.; Kulakov, M. Planar Twist Extrusion versus Twist Extrusion. *J. Mater. Process. Technol.* **2011**, *211*, 522–529. [CrossRef]

21. Beygelzimer, Y.; Reshetov, A.; Synkov, S.; Prokof'eva, O.; Kulagin, R. Kinematics of metal flow during twist extrusion investigated with a new experimental method. *J. Mater. Process. Technol.* **2009**, *209*, 3650 – 3656. [CrossRef]

22. Latypov, M.; Alexandrov, I.; Beygelzimer, Y.; Lee, S.; Kim, H. Finite element analysis of plastic deformation in twist extrusion. *Comput. Mater. Sci.* **2012**, *60*, 194–200. [CrossRef]

23. Maulidi, M.; Miyamoto, H.; Yuasa, M. Grain Refinement of Pure Magnesium Using Nonlinear Twist Extrusion. *Mater. Sci. Forum* **2018**, *939*, 54–62. [CrossRef]

24. Fang, N. A New Quantitative Sensitivity Analysis of the Flow Stress of 18 Engineering Materials in Machining. *J. Eng. Mater. Technol.* **2005**, *127*, 192–196. [CrossRef]

25. Mousavi, S.A.; Shahab, A.R.; Mastoori, M. Computational study of Ti–6Al–4V flow behaviors during the twist extrusion process. *Mater. Des.* **2008**, *29*, 1316–1329. [CrossRef]

26. Mousavi, S.A.; Shahab, A.R.; Mastoori, M. Numerical and experimental studies of the plastic strains distribution using subsequent direct extrusion after three twist extrusion passes. *Mater. Sci. Eng. A* **2010**, *527*, 3967–3974. [CrossRef]

27. Marat, I.; Latypov, Y.B.; Kim, H.S. Comparative Analysis of Two Twist-Based SPD Processes: Elliptical Cross-Section Spiral Equal-Channel Extrusion vs. Twist Extrusion. *Mater. Trans.* **2013**, *54*, 1587–1591.

28. Marat, I.; Latypov, Y.B.; Kim, H.S. Finite element analysis of the plastic deformation in tandem process of simple shear extrusion and twist extrusion. *Mater. Des.* **2015**, *83*, 858–865.

29. Lyszkowski, R.; Polkowski, W.; Czujko, T. Severe Plastic Deformation of Fe-22Al-5Cr Alloy by Cross-Channel Extrusion with Back Pressure. *Materials* **2018**, *11*, 2214. [CrossRef] [PubMed]